Article

Femtoscopy with identified hadrons in pp, pPb, and PbPb collisions in CMS

Ferenc Siklér [1] [iD] **for the CMS Collaboration**

[1]   Wigner RCP, Budapest; sikler.ferenc@wigner.mta.hu

Abstract: Short range correlations of identified charged hadrons in pp ($\sqrt{s}$ = 0.9, 2.76, and 7 TeV), pPb ($\sqrt{s_{NN}}$ = 5.02 TeV), and peripheral PbPb collisions ($\sqrt{s_{NN}}$ = 2.76 TeV) are studied with the CMS detector at the LHC. Charged pions, kaons, and protons at low momentum and in laboratory pseudorapidity $|\eta| < 1$ are identified via their energy loss in the silicon tracker. The two-particle correlation functions show effects of quantum statistics, Coulomb interaction, and also indicate the role of multi-body resonance decays and mini-jets. The characteristics of the one-, two-, and three-dimensional correlation functions are studied as a function of transverse pair momentum, k_T, and the charged-particle multiplicity of the event. The extracted radii are in the range 1-5 fm, reaching highest values for very high multiplicity pPb, also for similar multiplicity PbPb collisions, and decrease with increasing k_T. The dependence of radii on multiplicity and k_T largely factorizes and appears to be insensitive to the type of the colliding system and center-of-mass energy.

1. Introduction

Measurements of the correlation between hadrons emitted in high energy collisions of nucleons and nuclei can be used to study the spatial extent and shape of the created system. The characteristic radii, the homogeneity lengths, of the particle emitting source can be extracted with reasonable precision [1]. The topic of quantum correlations was well researched in the past by the CMS Collaboration [2,3] using unidentified charged hadrons produced in $\sqrt{s}$ = 0.9, 2.36, and 7 TeV pp collisions. Those studies only included one-dimensional fits (q_{inv}) of the correlation function. Our aim was to look for effects present in pp, pPb, and PbPb interactions using the same analysis methods, producing results as a function of the transverse pair momentum k_T and of the fully corrected charged-particle multiplicity N_{tracks} (in $|\eta| < 2.4$) of the event. In addition, not only charged pions, but also charged kaons are studied. All details of the analysis are given in Ref. [4].

2. Data analysis

The analysis methods (event selection, reconstruction of charged particles in the silicon tracker, finding interaction vertices, treatment of pile-up) are identical to the ones used in the previous CMS papers on the spectra of identified charged hadrons produced in $\sqrt{s}$ = 0.9, 2.76, and 7 TeV pp [5] and $\sqrt{s_{NN}}$ = 5.02 TeV pPb collisions [6]. A detailed description of the CMS detector can be found in Ref. [7].

For the present study 8.97, 9.62, and 6.20 M minimum bias events are used from pp collisions at $\sqrt{s}$ = 0.9 TeV, 2.76 TeV, and 7 TeV, respectively, while 8.95 M minimum bias events are available from pPb collisions at $\sqrt{s_{NN}}$ = 5.02 TeV. The data samples are completed by 3.07 M peripheral (60–100%) PbPb events, where 100% corresponds to fully peripheral, 0% means fully central (head-on) collision. The centrality percentages for PbPb are determined via measuring the sum of the energies in the forward calorimeters.

The multiplicity of reconstructed tracks, N_{rec}, is obtained in the region $|\eta| < 2.4$. Over the range 0 < N_{rec} < 240, the events were divided into 24 classes, a region that is well covered by the 60–100%
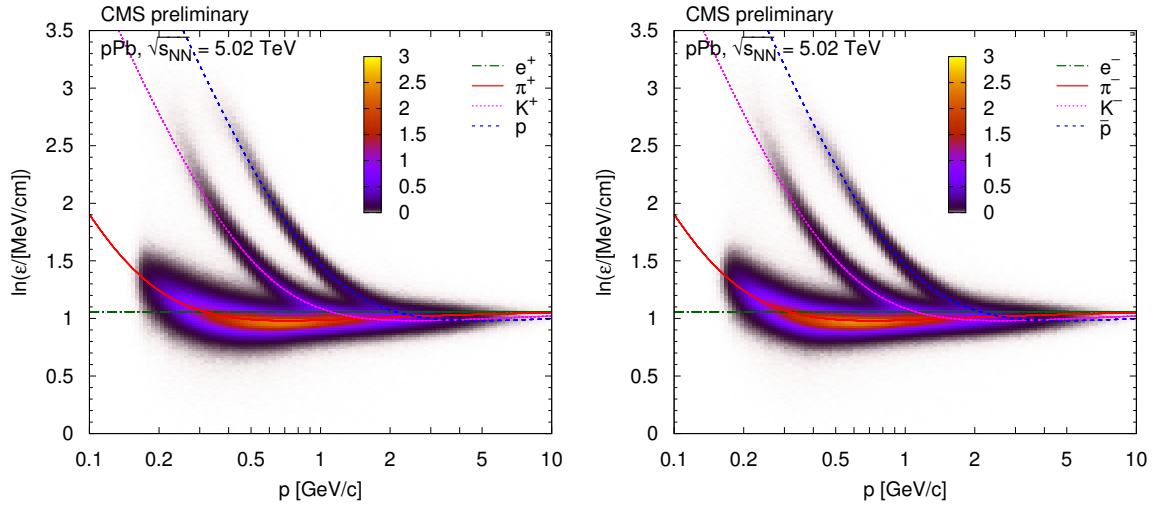
Figure 1. The distribution of $\ln \varepsilon$ as a function of total momentum p, for positively (left) and negatively (right) charged particles, in case of pPb collisions at $\sqrt{s_{NN}} = 5.02$ TeV [4]. Here ε is the most probable energy loss rate at a reference path length $l_0 = 450\ \mu$m. The z scale is shown in arbitrary units and is linear. The curves show the expected $\ln \varepsilon$ for electrons, pions, kaons, and protons (full theoretical calculation, Eq. (30.11) in Ref. [8]).

centrality PbPb collisions. To facilitate comparisons with models, the corresponding corrected charged particle multiplicity N_{tracks} in the same acceptance of $|\eta| < 2.4$ is also determined.

The reconstruction of charged particles in CMS is bounded by the acceptance of the tracker and by the decreasing tracking efficiency at low momentum. Particle-by-particle identification using specific ionization is possible in the momentum range $p < 0.15$ GeV/c for electrons, $p < 1.15$ GeV/c for pions and kaons, and $p < 2.00$ GeV/c for protons (Fig. 1). In view of the (η, p_{T}) regions where pions, kaons, and protons can all be identified, only particles in the band $-1 < \eta < 1$ (in the laboratory frame) were used for this measurement. In this analysis a very high purity ($> 99.5\%$) particle identification is required, ensuring that less than 1% of the examined particle pairs would be fake.

2.1. Correlations

The pair distributions are binned in the number of reconstructed charged particles N_{rec} of the event, in the transverse pair momentum $k_{\text{T}} = |\mathbf{p_{T,1}} + \mathbf{p_{T,2}}|/2$, and also in the relative momentum ($\mathbf{q}$) variables in the longitudinally co-moving system of the pair. One-dimensional ($q_{\text{inv}} = |\mathbf{q}|$), two-dimensional ($q_l, q_t$), and three-dimensional (q_l, q_o, q_s) analyses are performed. Here q_o is the component of $\mathbf{q_t}$ parallel to $\mathbf{k_T}$, q_s is the component of $\mathbf{q_t}$ perpendicular to $\mathbf{k_T}$.

The construction of the $\mathbf{q}$ distribution for the "signal" pairs is straightforward: all valid particle pairs from the same event are taken and the corresponding histograms are filled. There are several choices for the construction of the background. We considered the following three prescriptions:

- particles from the actual event are paired with particles from some given number of, in our case 25, preceding events ("event mixing"); only events belonging to the same multiplicity (N_{rec}) class are mixed;
- particles from the actual event are paired, the laboratory momentum vector of the second particle is rotated around the beam axis by 90 degrees ("rotated");
- particles from the actual event are paired, but the laboratory momentum vector of the second particle is negated ("mirrored").

Based on the goodness-of-fit distributions the event mixing prescription was used while the rotated and mirrored versions, which give worse or much worse χ^2/ndf values, were employed in the estimation of the systematic uncertainty.

The measured two-particle correlation function $C_2(\mathbf{q})$ is the ratio of signal and background distributions

$$C_2(\mathbf{q}) = \frac{N_{\text{signal}}(\mathbf{q})}{N_{\text{bckgnd}}(\mathbf{q})}, \tag{1}$$

where the background is normalized such that it has the same integral as the signal distribution. The quantum correlation function C_{BE}, part of C_2, is the Fourier transform of the source density distribution $f(\mathbf{r})$. There are several possible functional forms that are commonly used to fit C_{BE} present in the data: Gaussian $(1 + \lambda \exp\left[-(qR)^2/(\hbar c)^2\right])$ and exponential parametrizations $(1 + \lambda \exp\left[-(|q|R)/(\hbar c)\right])$, and a mixture of those in higher dimensions. (The denominator $\hbar c = 0.197$ GeV fm is usually omitted from the formulas, we will also do that in the following.) Factorized forms are particularly popular, such as $\exp(-q_l^2 R_l^2 - q_o^2 R_o^2 - q_s^2 R_s^2)$ or $\exp(-q_l R_l - q_o R_o - q_s R_s)$ with some theoretical motivation. The fit parameters are usually interpreted as chaoticity λ, and characteristic radii R, the homogeneity lengths, of the particle emitting source.

As will be shown in Sec. 3, the exponential parametrization does a very good job in describing all our data. It corresponds to the Cauchy (Lorentz) type source distribution $f(r) = R/(2\pi^2\left[r^2 + (R/2)^2\right]^2)$. Theoretical studies show that for the class of stable distributions, with index of stability $0 < \alpha \leq 2$, the Bose-Einstein correlation function has a stretched exponential shape [9,10]. The exponential correlation function implies $\alpha = 1$. (The Gaussian would correspond to the special case of $\alpha = 2$.) The forms used for the fits are

$$C_{\text{BE}}(q_{\text{inv}}) = 1 + \lambda \exp\left[-q_{\text{inv}}R\right], \tag{2}$$

$$C_{\text{BE}}(q_l, q_t) = 1 + \lambda \exp\left[-\sqrt{(q_l R_l)^2 + (q_t R_t)^2}\right], \tag{3}$$

$$C_{\text{BE}}(q_l, q_o, q_s) = 1 + \lambda \exp\left[-\sqrt{(q_l R_l)^2 + (q_o R_o)^2 + (q_s R_s)^2}\right], \tag{4}$$

meaning that the system in multi-dimensions is an ellipsoid with differing radii R_l, R_t, or R_l, R_o, and R_s.

2.2. Coulomb interaction

After the removal of the trivial phase space effects (ratio of signal and background distributions), one of the most important source of correlations is the mutual Coulomb interaction of the emitted charged particles. The effect of the Coulomb interaction is taken into account by the factor K, the squared average of the relative wave function Ψ, as $K(q_{\text{inv}}) = \int d^3\mathbf{r}\, f(\mathbf{r})\, |\Psi(\mathbf{k}, \mathbf{r})|^2$, where $f(\mathbf{r})$ is the source intensity discussed above. For pointlike source, $f(\mathbf{r}) = \delta(\mathbf{r})$, and we get the Gamow factor $G(\eta) = |\Psi(0)|^2 = 2\pi\eta/[\exp(2\pi\eta) - 1]$, where $\eta = \pm\alpha m/q_{\text{inv}}$ is the Landau parameter, α is the fine-structure constant, m is the mass of the particle. The positive sign should be used for repulsion, and the negative is for attraction.

For an extended source, a more elaborate treatment is needed [11]. The use of the Bowler-Sinyukov formula [12,13] is popular. Our data on unlike-sign correlation functions show that while the Gamow factor might give a reasonable description of the Coulomb interaction for pions, it is clearly not enough for kaons. In the q range studied in this analysis $\eta \ll 1$ applies. The absolute square of confluent hypergeometric function of the first kind F, present in Ψ, can be well approximated as $|F|^2 \approx 1 + 2\eta\,\text{Si}(x)$ where Si is the sine integral function. Furthermore, for Cauchy type source functions the factor K is nicely described by the formula $K(q_{\text{inv}}) = G(\eta)\left[1 + \pi\eta q_{\text{inv}}R/(1.26 + q_{\text{inv}}R)\right]$. In the last step we substituted $q_{\text{inv}} = 2k$. The factor π in the approximation comes from the fact that for large kr arguments $\text{Si}(kr) \to \pi/2$. Otherwise it is a simple but faithful approximation of the result of a numerical calculation, with deviations less than 0.5%.
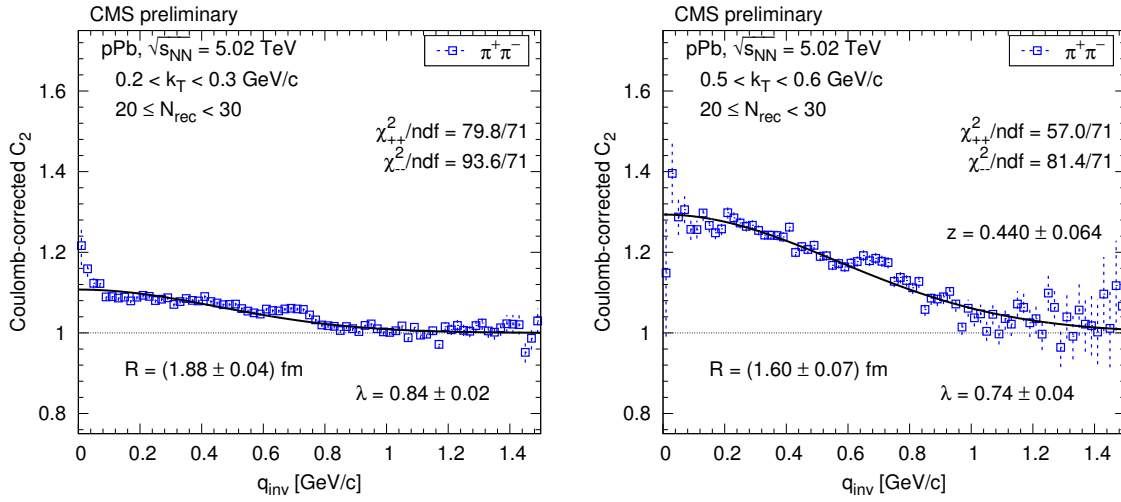
Figure 2. Contribution of clusters (mini-jets and multi-body decays of resonances) to the measured Coulomb-corrected correlation function of $\pi^+\pi^-$ (open squares) for some selected k_T bins, $20 \leq N_{rec} < 30$, in case of pPb interactions at $\sqrt{s_{NN}} = 5.02$ TeV [4]. The solid curves show the result of the Gaussian fit.

2.3. Clusters: mini-jets, multi-body decays of resonances

The measured unlike-sign correlation functions show contributions from various resonances. The seen resonances include the K_S^0, the $\rho(770)$, the $f_0(980)$, the $f_2(1270)$ decaying to $\ss^+\ss^-$, and the $\phi(1020)$ decaying to K^+K^-. Also, e^+e^- pairs from γ conversions, when misidentified as pion pairs, can appear as a very low q_{inv} peak in the $\pi^+\pi^-$ spectrum. With increasing N_{rec} values the effect of resonances diminishes, since their contribution is quickly exceeded by the combinatorics of unrelated particles.

Nevertheless, the Coulomb-corrected unlike-sign correlation functions are not always close to unity at low q_{inv}, but show a Gaussian-like hump (Fig. 2). That structure has a varying amplitude but a stable scale (σ of the corresponding Gaussian) of about 0.4 GeV/c. This feature is often related to particles emitted inside low momentum mini-jets, but can be also attributed to the effect of multi-body decays of resonances. In the following we will refer to those possibilities as fragmentation of clusters, or cluster contribution. We have fitted the one-dimensional unlike-sign correlation functions with a (N_{rec}, k_T)-dependent Gaussian parametrization [4].

The cluster contribution can be also extracted in the case of a like-sign correlation function, if the momentum scale of the Bose-Einstein correlation and that of the cluster contribution (≈ 0.4 GeV/c) are different enough. An important element in both mini-jet and multi-body resonance decays is the conservation of electric charge that results in a stronger correlation for unlike-sign pairs than for like-sign pairs. Hence the cluster contribution is expected to be also present for like-sign pairs, with similar shape but a somewhat smaller amplitude. The form of the cluster-related contribution obtained from unlike-sign pairs, but now multiplied by the extracted relative amplitude z, is used to fit the like-sign correlations. A selection of correlation functions and fits are shown in Figs. 3 and 4.

In the case of two and three dimensions the measured unlike-sign correlation functions show that instead of q_{inv}, the length of the weighted sum of **q** components is a better common variable.
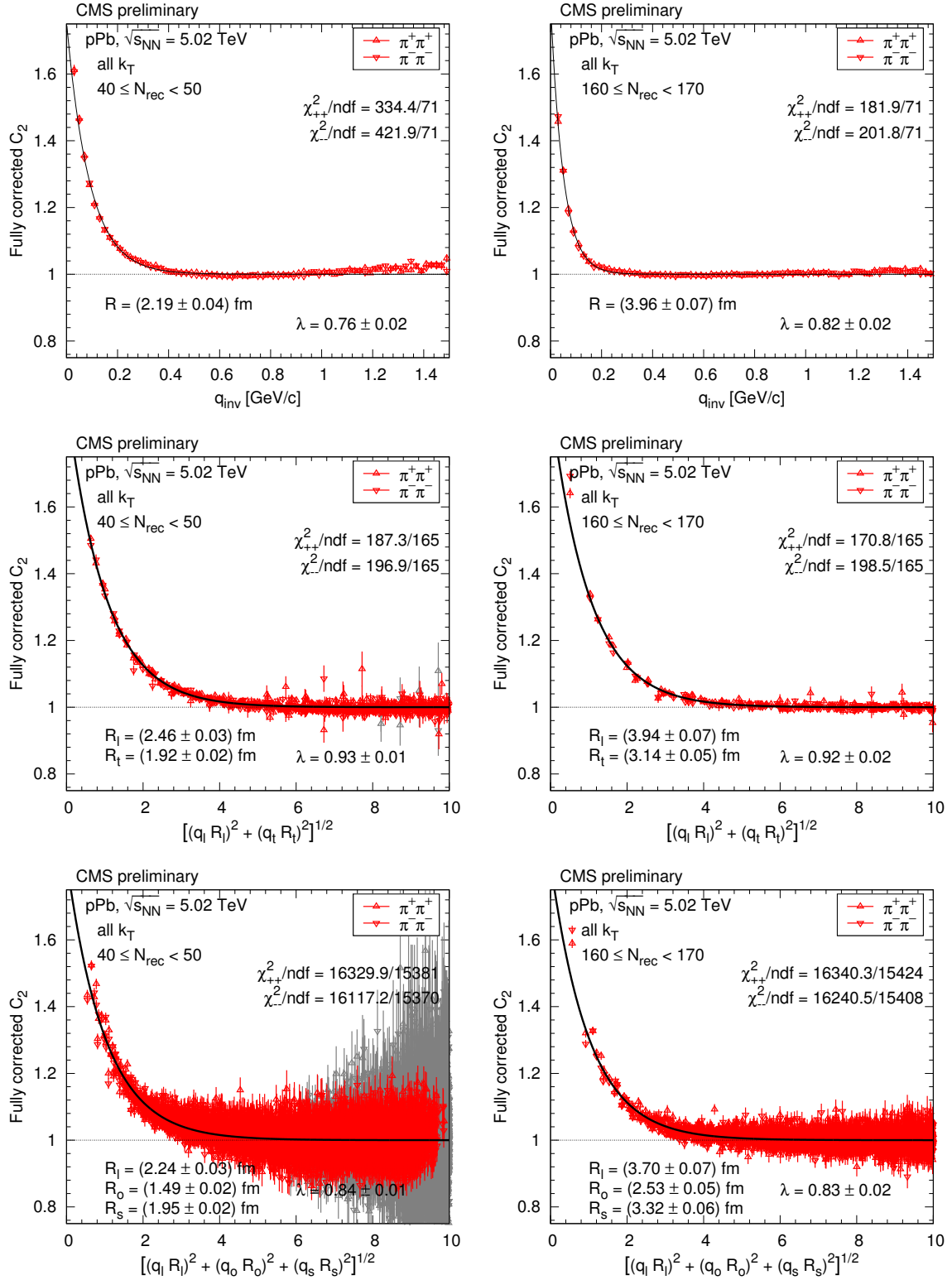
Figure 3. The like-sign correlation function of pions (red triangles) corrected for Coulomb interaction and cluster contribution (mini-jets and multi-body resonance decays) as a function of q_{inv} or the combined momentum, in some selected N_{rec} bins for all k_T [4]. The solid curves indicate fits with the exponential Bose-Einstein parametrization.
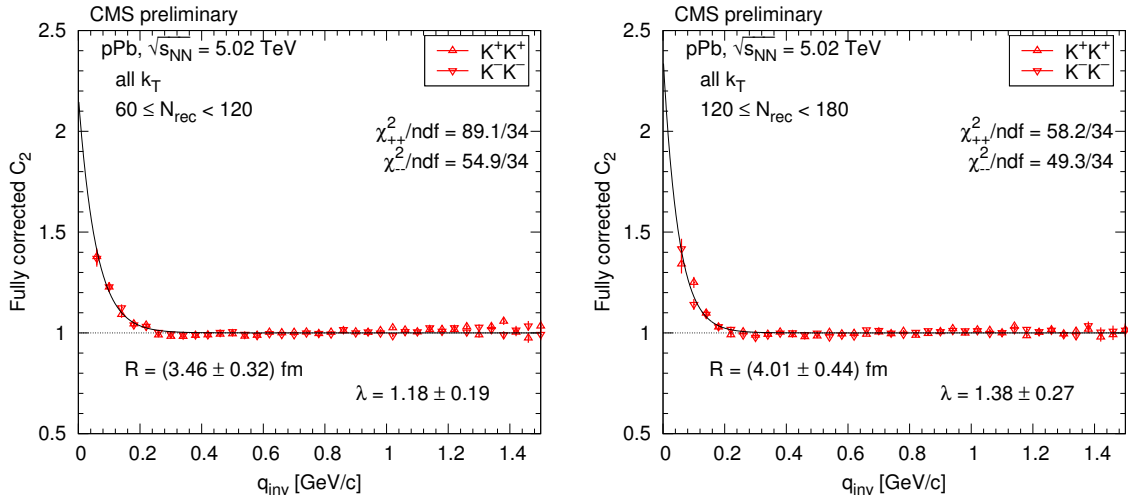
Figure 4. The like-sign correlation function of kaons (red triangles) corrected for Coulomb interaction and cluster contribution (mini-jets and multi-body resonance decays) as a function of q_{inv}, in some selected N_{rec} bins for all k_T [4]. The solid curves indicate fits with the Bose-Einstein parametrization.

3. Results

The systematic uncertainties are dominated by two sources: the dependence of the final results on the way the background distribution is constructed, and the uncertainties of the amplitude z of the cluster contribution for like-sign pairs with respect to those for unlike-sign ones.

The characteristics of the extracted one- and two-dimensional correlation functions as a function of the transverse pair momentum k_T and of the charged-particle multiplicity N_{tracks} (in the range $|\eta| <$ 2.4 in the laboratory frame) of the event are presented here. Three-dimensional results are detailed in Ref. [4]. In all the following plots (Figs. 5–7), the results of positively and negatively charged hadrons are averaged. For clarity, values and uncertainties of the neighboring N_{tracks} bins were averaged two by two, and only the averages are plotted. The central values of radii and chaoticity parameter λ are given by markers. The statistical uncertainties are indicated by vertical error bars, the combined systematic uncertainties (choice of background method; uncertainty of the relative amplitude z of the cluster contribution; low q exclusion) are given by open boxes. Unless indicated, the lines are drawn to guide the eye (cubic splines whose coefficients are found by weighing the data points with the inverse of their squared statistical uncertainty).

The extracted exponential radii for pions increase with increasing N_{tracks} for all systems and center-of-mass energies studied, for one, two, and three dimensions alike. Their values are in the range 1–5 fm, reaching highest values for very high multiplicity pPb, also for similar multiplicity PbPb collisions. The N_{tracks} dependence of R_l and R_t is similar for pp and pPb in all k_T bins, and that similarity also applies to peripheral PbPb if $k_T > 0.4$ GeV/c. In general there is an ordering, $R_l > R_t$, and $R_l > R_s > R_o$, thus the pp and pPb source is elongated in the beam direction. In the case of peripheral PbPb the source is quite symmetric, and shows a slightly different N_{tracks} dependence, with largest differences for R_t and R_o, while there is a good agreement for R_l and R_s. The most visible divergence between pp, pPb and PbPb is seen in R_o that could point to the differing lifetime of the created systems in those collisions.

The kaon radii also indicate some increase with N_{tracks} (not shown), although its magnitude is smaller than that for pions. Longer lived resonances and rescattering may play a role here.
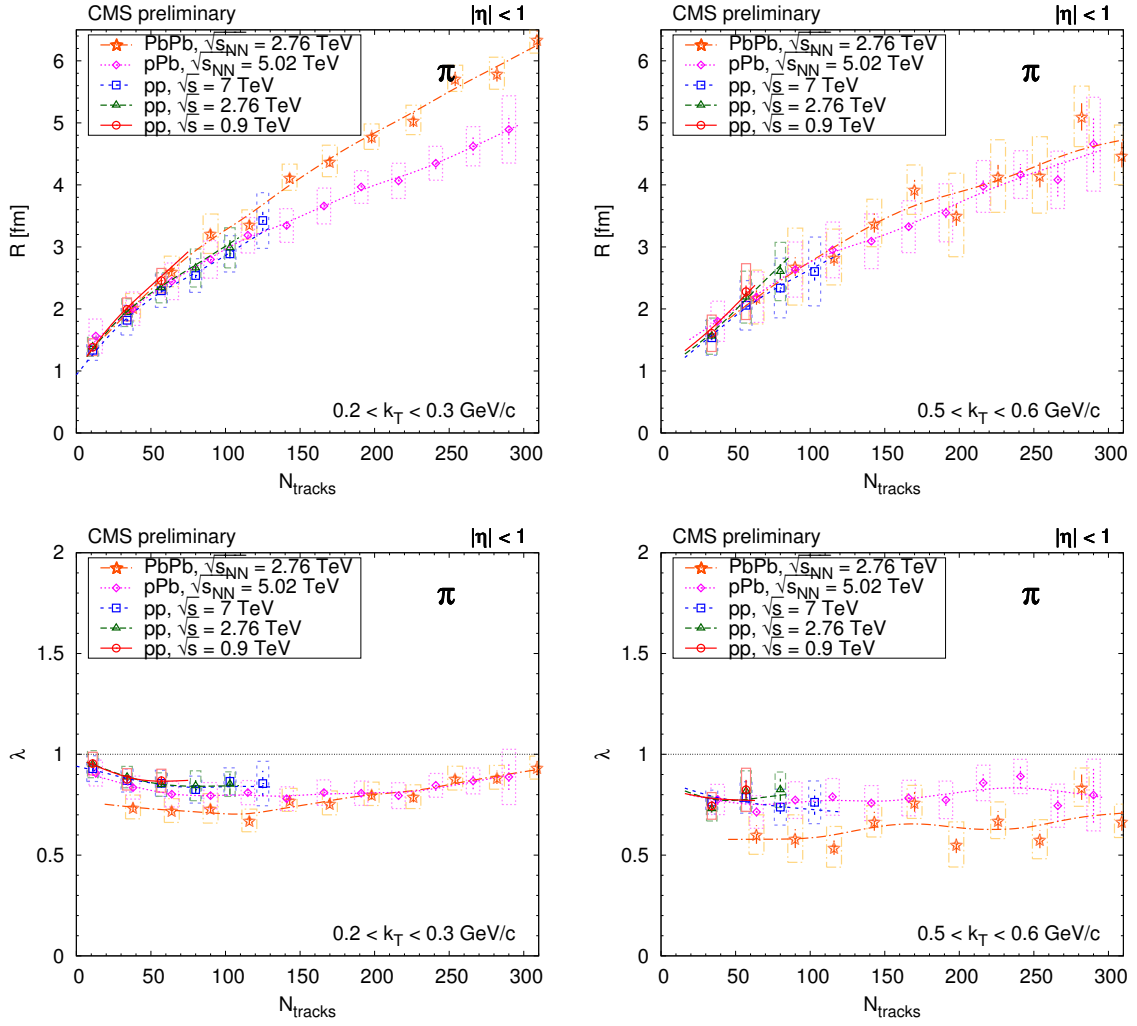
Figure 5. The N_{tracks} dependence of the one-dimensional pion radius (top) and the one-dimensional pion chaoticity parameter (bottom), shown here for several k_T bins, for all studied reactions [4]. Lines are drawn to guide the eye.
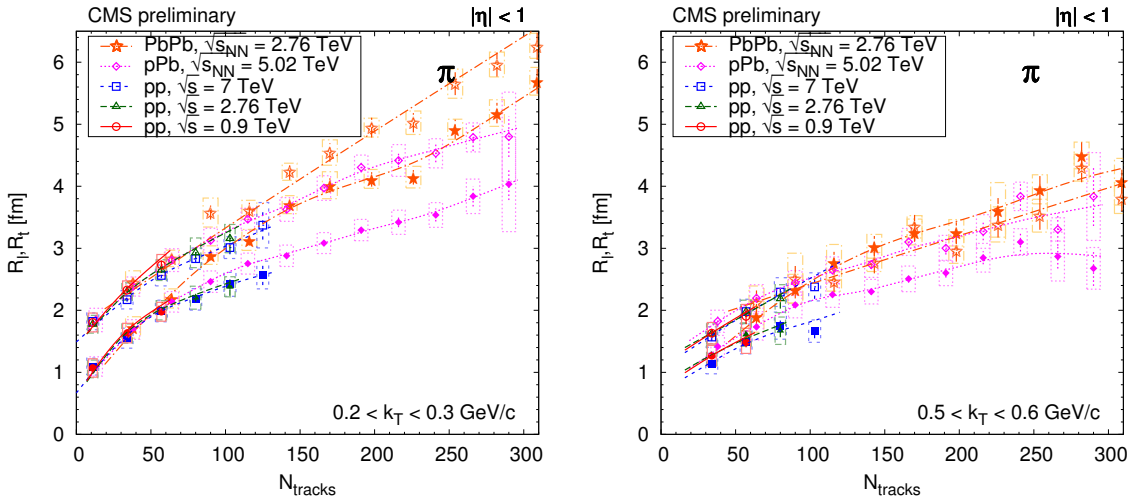

Figure 6. The N_{tracks} dependence of the two-dimensional pion radii (R_l – open symbols, R_t – closed symbols), shown here for several k_T bins, for all studied reactions [4]. Lines are drawn to guide the eye.

3.1. Scaling

The extracted radii are in the range 1–5 fm, reaching highest values for very high multiplicity pPb, also for similar multiplicity PbPb collisions, and decrease with increasing k_T. By fitting the radii with a product of two independent functions of N_{tracks} and k_T, the dependences on multiplicity and pair momentum appear to factorize. In some cases the radii are less sensitive to the type of the colliding system and center-of-mass energy. Radius parameters as a function of N_{tracks} at $k_T = 0.45\,\text{GeV}/c$ are shown in the left column of Fig. 7. We have also fitted and plotted the following R_{param} functions

$$R_{param}(N_{tracks}, k_T) = \left[a^2 + (bN_{tracks}^{\beta})^2\right]^{1/2} \cdot (0.2\,\text{GeV}/c/k_T)^{\gamma}, \tag{5}$$

where the minimal radius a and the exponents γ of k_T are kept the same for a given radius component, for all collision types. This choice of parametrization is based on previous results [14]. The minimal radius can be connected to the size of the proton, while the power-law dependence on N_{tracks} is often attributed to the freeze-out density of hadrons. The ratio of radius parameter and the value of the above parametrization at $k_T = 0.45\,\text{GeV}/c$ as a function k_T is shown in the right column of Fig. 7.

4. Conclusions

The similarities observed in the N_{tracks} dependence may point to a common critical hadron density in pp, pPb, and peripheral PbPb collisions, since the present correlation technique measures the characteristic size of the system near the time of the last interactions.

References

1. Erazmus, B.; Lednicky, R.; Martin, L.; Nouais, D.; Pluta, J. Nuclear interferometry from low-energy to ultrarelativistic nucleus-nucleus collisions. SUBATECH-96-03.
2. CMS Collaboration. Measurement of Bose-Einstein correlations with first CMS data. *Phys. Rev. Lett.* **2010**, *105*, 032001, [arXiv:hep-ex/1005.3294].
3. CMS Collaboration. Measurement of Bose-Einstein Correlations in *pp* Collisions at $\sqrt{s} = 0.9$ and 7 TeV. *JHEP* **2011**, *05*, 029, [arXiv:hep-ex/1101.3518].
4. CMS Collaboration. Femtoscopy with identified charged hadrons in pp, pPb, and peripheral PbPb collisions at LHC energies. *CMS* **2014**, *PAS HIN-14-013*.
5. CMS Collaboration. Study of the inclusive production of charged pions, kaons, and protons in *pp* collisions at $\sqrt{s} = 0.9$, 2.76, and 7 TeV. *Eur. Phys. J. C* **2012**, *72*, 2164, [arXiv:hep-ex/1207.4724].
6. CMS Collaboration. Study of the production of charged pions, kaons, and protons in pPb collisions at $\sqrt{s_{NN}} = 5.02$ TeV. *Eur. Phys. J. C* **2014**, *74*, 2847, [arXiv:hep-ex/1307.3442].
7. CMS Collaboration. The CMS experiment at the CERN LHC. *JINST* **2008**, *3*, S08004.
8. Particle Data Group.; Beringer, J.; others. Review of Particle Physics. *Phys. Rev. D* **2012**, *86*, 010001.
9. Csörgő, T.; Hegyi, S.; Zajc, W. Bose-Einstein correlations for Levy stable source distributions. *Eur. Phys. J. C* **2004**, *36*, 67, [arXiv:nucl-th/nucl-th/0310042].
10. Csörgő, T.; Hegyi, S.; Zajc, W. Stable Bose-Einstein correlations **2004**. [arXiv:nucl-th/nucl-th/0402035].
11. Pratt, S. Coherence and Coulomb effects on pion interferometry. *Phys. Rev. D* **1986**, *33*, 72.
12. Bowler, M. Coulomb corrections to Bose-Einstein correlations have been greatly exaggerated. *Phys. Lett. B* **1991**, *270*, 69–74.
13. Sinyukov, Y.; Lednicky, R.; Akkelin, S.; Pluta, J.; Erazmus, B. Coulomb corrections for interferometry analysis of expanding hadron systems. *Phys. Lett. B* **1998**, *432*, 248.
14. Lisa, M. Femtoscopy in heavy ion collisions: Wherefore, whence, and whither? *AIP Conf. Proc.* **2006**, *828*, 226, [arXiv:nucl-ex/nucl-ex/0512008].
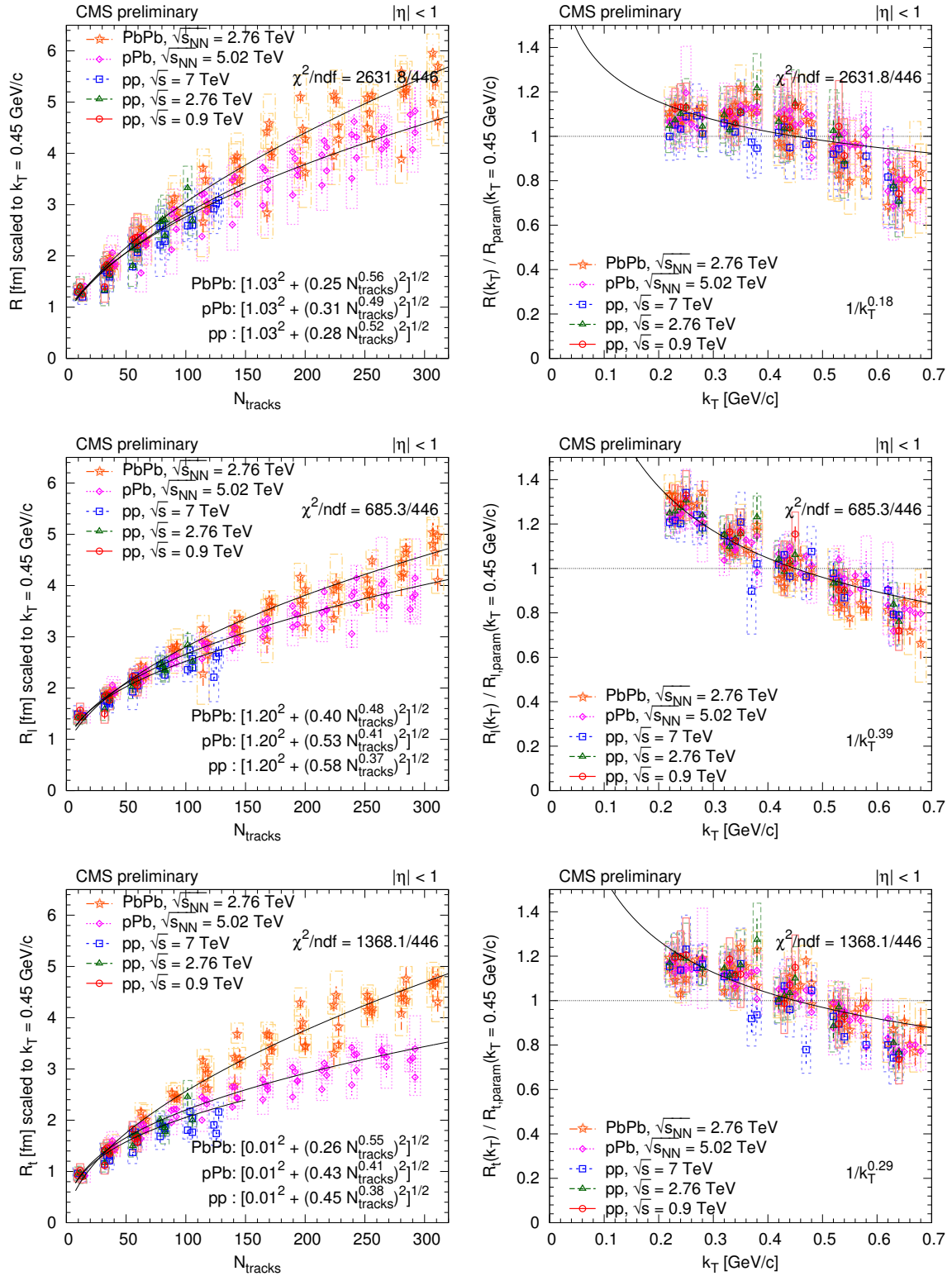
Figure 7. Left: radius parameters as a function of N_{tracks} scaled to $k_{\text{T}} = 0.45$ GeV/c with help of the parametrization R_{param} (Eq. (5)). Right: ratio of the radius parameter and the value of the parametrization R_{param} (Eq. (5)) at $k_{\text{T}} = 0.45$ GeV/c as a function of k_{T}. (Points were shifted to left and to right with respect to the center of the k_{T} bin for better visibility.) Upper row: R from the one-dimensional (q_{inv}) analysis. Middle row: R_l from the two-dimensional (q_l, q_t) analysis. Bottom row: R_t from the two-dimensional (q_l, q_t) analysis. Fit results are indicated in the figures [4], for details see text.